SPE 35159

Borehole Imaging The Future of Formation Evaluation

R.L. Sanders, SPE,and K.D. Fuchs, Halliburton Energy Services

This paper was prepared for presentation at the Permian Basin Oil & Gas Recovery Conference held in Midland, Texas 27-29 March 1996.

Abstract

The emerging technology of borehole imaging coupled with the advances in graphics software will shape the future of formation evaluation because (1) imaging reveals new opportunities for exploration in unconventional and previously neglected reservoirs,(2) imaging exhibits the complex distribution of porosity and permeability throughout the reservoir, and (3) imaging enhances the knowledge of the physical dynamics of the reservoir for improved stimulation techniques.

Introduction

Traditional methods of formation evaluation have relied upon the interpretation of data recorded from a wireline tool in the borehole. While no wireline tool directly measures the porosity or the resistivity of the formation, these properties have served as the basis for analysis of formations for some seventy years. The advantage of borehole imaging is the ability to visualize the many variations of porosity types, permeability, and lithology changes within the rock. Borehole imaging utilizes either acoustic or resistivity recording devices to graphically display the surface features of the borehole wall in the open hole environment. This paper presents only the resistivity based tool, the electrical micro-imaging tool as the source for the following case studies.

Tool Descriptions and Image Display

The electrical micro-imaging tool is a six arm pad device with twenty-five button electrodes mounted on each pad **(Fig. 1).** Each button electrode emits an electrical current into the formation for a distance of fifteen inches. The changes in the permeability, porosity and lithology of the formations near the borehole wall are reflected as resistivity variations in the electrical current return to the individual electrodes. A system of magnetometers references the tool's orientation to magnetic north. Utilizing a computer workstation, these resistivity variations are processed into a two dimensional image that represents the surface of the borehole wall with respect to magnetic north **(Fig. 2)**. The images are presented in either a gray-scale or color display with a standardized color code representing the variation in formation features. Low porosity, low permeability, and high resistivity features represent the light end of the color spectrum. The high porosity, permeable, and low resistivity events are scaled as the darker colors.

Unconventional Reservoirs

The electrical micro- imaging tool reveals many potential opportunities that are present in unconventional reservoirs but may be undetected using standard logging suites. An unconventional reservoir is described as a reservoir (1) where the presence of natural fractures is the primary reason for the hydrocarbon production, (2) the reservoir is not considered productive in the area, and (3) the completion of the well may require unconventional stimulation techniques.

An unconventional reservoir may be characterized by events occurring during the drilling of a well that may not be obvious on conventional logging suites. Examples of these events would be the incidence of oil on the mud pits, gas increases on the mud log, or unusual drilling breaks without any corresponding curve responses on the conventional logs. Each of these events taken individually may not be considered significant but the sum of all the events would be could be relevant in terms of a commercial discovery.

One area of interest in the Permian Basin is the Spraberry Trend. The majority of wells drilled in the Spraberry Trend

have traditionally used only gamma ray\neutron logs for the evaluation of the Spraberry zones. The gamma ray\neutron log is the primary logging suite for evaluating the Spraberry. However, the logging suite is inadequate in terms of analyzing the zones for hydrocarbon potential above the Spraberry. The Spraberry production is related to the presence of natural fracturing. The processes that generated fracturing in the Spraberry were also active in the post-Spraberry formations. Ref. 1 presents a comprehensive study of the geological activities that have caused the fracturing in the Spraberry Trend. In addition, Ref. 1 has examined the impact of natural fracturing on post-Spraberry formations.

The following case study demonstrates the manner in which the imaging tool is used to verify the presence of the fracture system in the Clearfork formation. During the drilling of the subject well, drilling breaks and background gas increases were recorded on the mud log in the zone of interest. While running the gamma ray\neutron\density log, the wireline log data showed the following responses (1) unusually high gamma ray responses, suggesting the presence of uranium plating on the fracture faces and (2) the unusual increase in the density porosity values in the zone of interest. The density anomalies were considered to be caused by fractures intersecting the borehole wall. These fractures will create an irregular surface on the wall resulting in the poor density pad contact. **Fig. 3** is a composite of the wireline well data merged with the mud log data.

In consideration of the match between drilling breaks, mud log shows, high gamma ray reading, and the density porosity increases all events suggested the well to be fractured in the zone of interest. **Fig. 4** shows the electrical micro-imaging display over the correlative interval. The imaging display shows the presence of natural fractures intersecting the wellbore in a northeast to southwest direction. Because of the presence of fracturing and the mud log shows, the well was cased and perforated. The well was tested in the fractured interval by perforating the zone and then acidizing with 500 gallons of 12% Hcl. The reservoir could have responded more positively to an open hole completion where the fractures would have had greater exposure to the proper stimulation techniques. At the present, an offset location is being considered with an open hole completion to follow if this zone is present in the offset well.

Complex Porosity Analysis

This example is from a Canyon Reef well in Howard County, Texas. The problem this operator needed to resolve was reconciling the net pay with the volume of hydrocarbons that are being produced. The reserve estimates, which were based upon the net footage of the pay zone, have been underestimating the actual production results. The subject well was drilled and logged with a conventional logging suite **(Fig. 5)**. The open hole logs show a porosity break at 8614' - 8618'. This productive zone is comparable to correlative zones in other wells in the area characterized by the thin interval of porosity. Several drill stem tests have been run in adjacent wells that predicted very favorable production. A borehole imaging tool was run to view any abnormal porosity structure that the conventional logs did not detect. **Fig. 6** is a display of the electrical micro-imaging log that reveals the intricate porosity system. The matrix porosity is clearly evident as the darker band of material on the borehole image. The imaging display shows a complex network of secondary porosity that will contribute to the productive capacity of the well. This interconnected network of porosity is undetected by the standard neutron\density log. This system of secondary porosity was undetected on the standard logging suite in this well and other wells in the area. For this reason, the wells in this area outperformed the original estimates that were based upon the standard logging measurements.

The porosity and resistivity devices are not producing erroneous numbers. These standard logging suites simply lack the resolution to measure the subtle changes in the formations. The electrical micro-imaging tool provides an image resolution of approximately .2 of an inch. In addition, one result of imaging complex porosity networks is the ability to describe and compute a relative measure of the porosity system. Imaging logs have previously been used for the evaluation of thinly laminated shaly sand reservoirs. Ref. 2 documents the methods of deriving quantitative resistivity measurements from the imaging tools.

The following example is from a well drilled into the Clearfork formation in Ector County, Texas. **Fig. 7** shows a composite log comparing the neutron\density crossplot porosity to the sonic porosity over a selected interval of the wellbore. The mean value of the neutron\density crossplot porosity is twice the value of the mean sonic porosity. It is generally considered that the neutron and density tools measure total porosity while the sonic tool measures the matrix porosity. This difference in porosity values would then indicate that the presence of secondary porosity is the cause for the greater porosity values from the neutron\density porosity compared to the sonic porosity values. **Fig. 8** shows the electrical micro-image log of the zone of interest in the subject well. Not only is the matrix porosity visible, but also visible on the image are both vugular and fracture porosity. In addition to the standard borehole image, the resistivity response of the middle button electrode on the number one pad is plotted adjacent to the image. This resistivity measurement is a function of the formation water resistivity, mud resistivity, and pore geometry of the formation adjacent to the button electrode. A porosity index that is derived from the resistivity reading of the imaging tool can be calculated for each sampled interval. These resistivity derived porosities can then be compared with the standard porosity values. The cementation exponent used in the water saturation

equations may then be refined in consideration of these resistivity derived porosities.

Conclusions

The use of conventional logging programs has provided the traditional approach for evaluating formations in the past. One progressive step in the evolution of conventional logging programs was the use of the gamma\neutron\density log to replace the regular gamma\neutron. The next step in the process will be the addition of borehole imaging tools. With the numerous applications inherent to the imaging tools, these tools will become an integral part of future logging programs.

References

1. Winfree, K.E.: "Post-Permian Folding and Fracturing of the Spraberry and San Andres Formations within the Midland Basin of West Texas", *West Texas Geological Society Publication 94-95*, 189.
2. Fam, M.Y. et.al.: "Applying Electrical Micro-Imaging Logs to Reservoir Characterization", paper SPE 30608 presented at the 1995 SPE Annual Technical Conference and Exhibition, Dallas, Oct. 22-25.

SPECIFICATIONS FOR MICRO IMAGING TOOL

Length:	**39.5 ft**
Weight:	**500 lb**
Diameter:	**5.0 in**
Maximum Temperature:	**350 degF**
Maximum Pressure:	**20,000 psi**
Resolution:	**0.2 in**
Depth of investigation:	**30 in**
Minimum Hole Size:	**6.25 in**
Maximum Hole Size:	**21 in**
Number of Buttons:	**150**
Number of Pads:	**6**

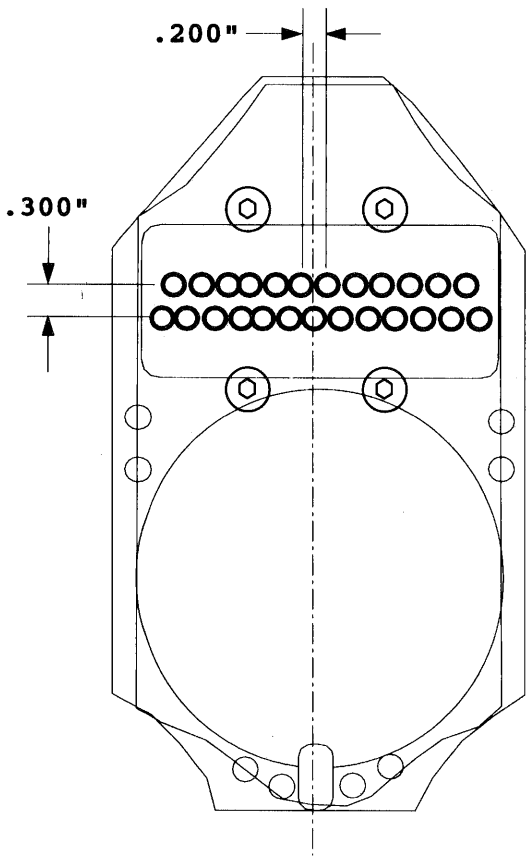

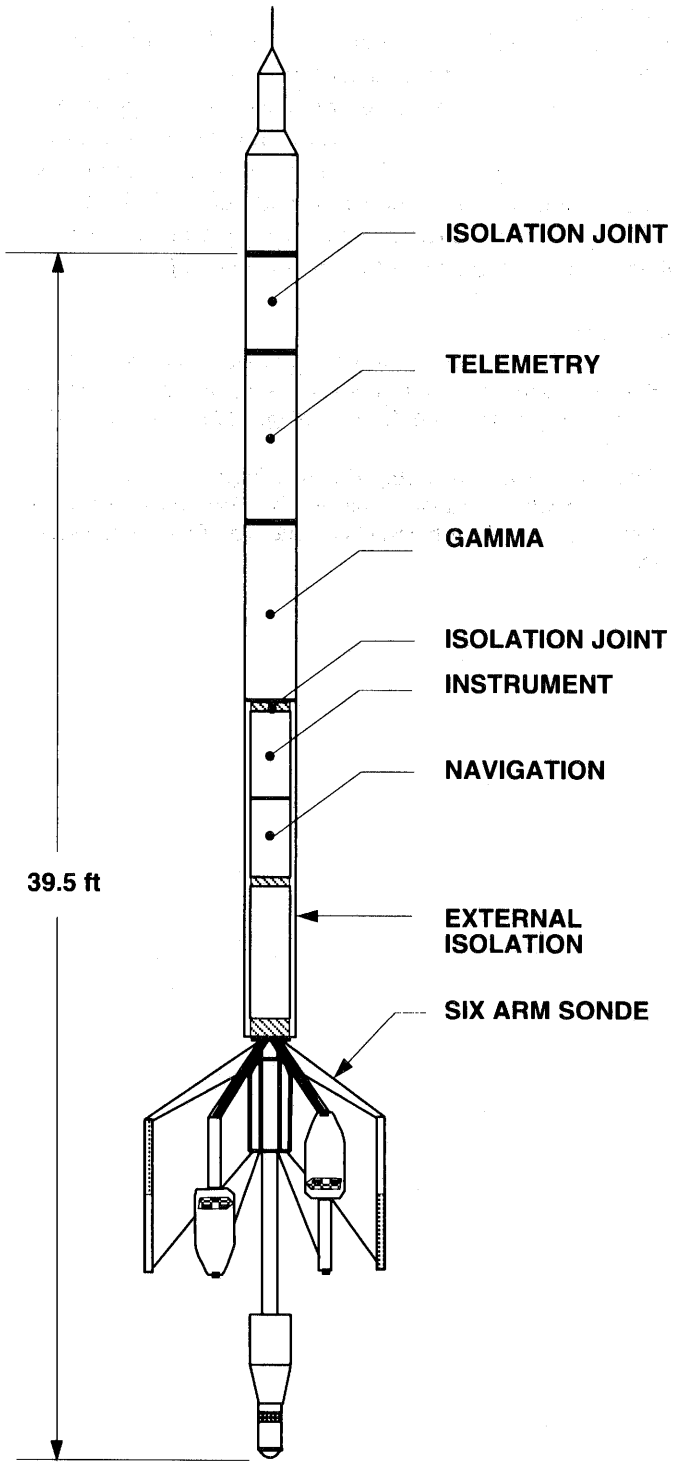

Fig. 1 The electrical micro-imaging tool has six arms, 39.5 feet in length, and can be run in a wellbore as small as 6.25 inches.

EMI grayscale representation of geological features.

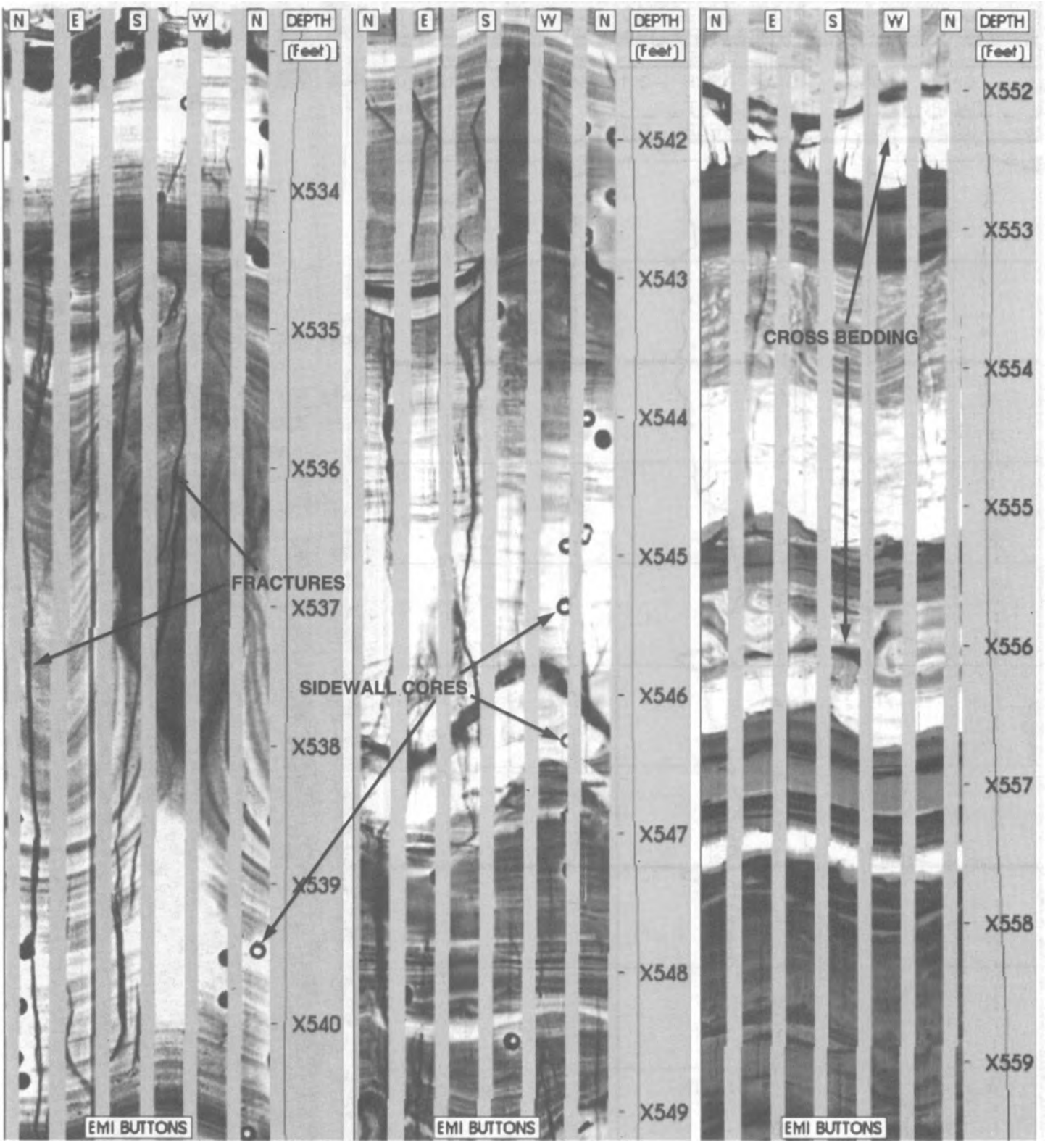

Fig. 2 Darker colors represent high porosity, high permeable, and low resistivity events. Lighter colors represent low porosity,low permeablity, and high resistivty events.

Density/Neutron of the Clearfork formation.

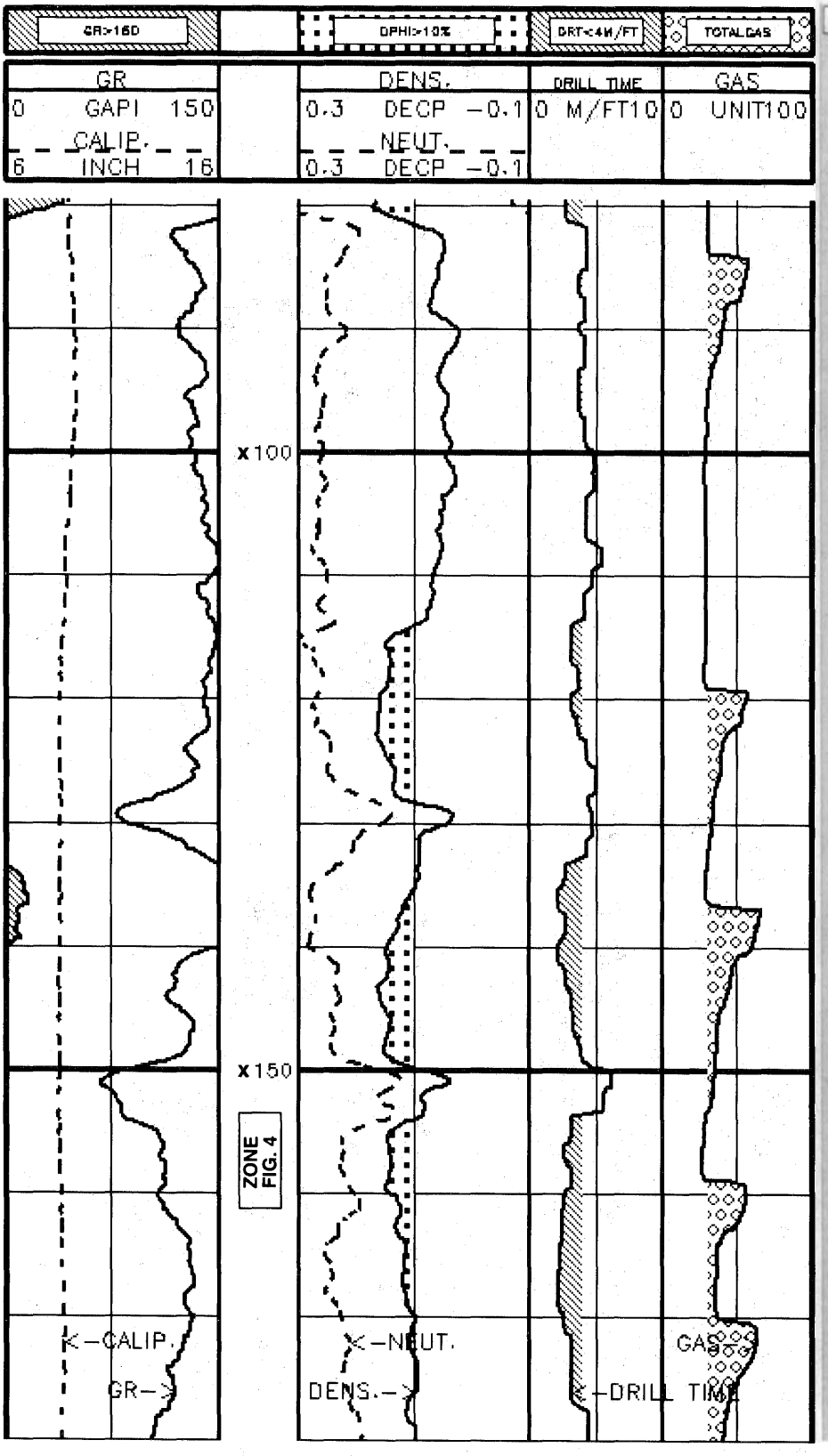

Fig. 3 Composite of the wireline well data merged with the mud log data.

EMI display of natural fractures in NE/SW direction

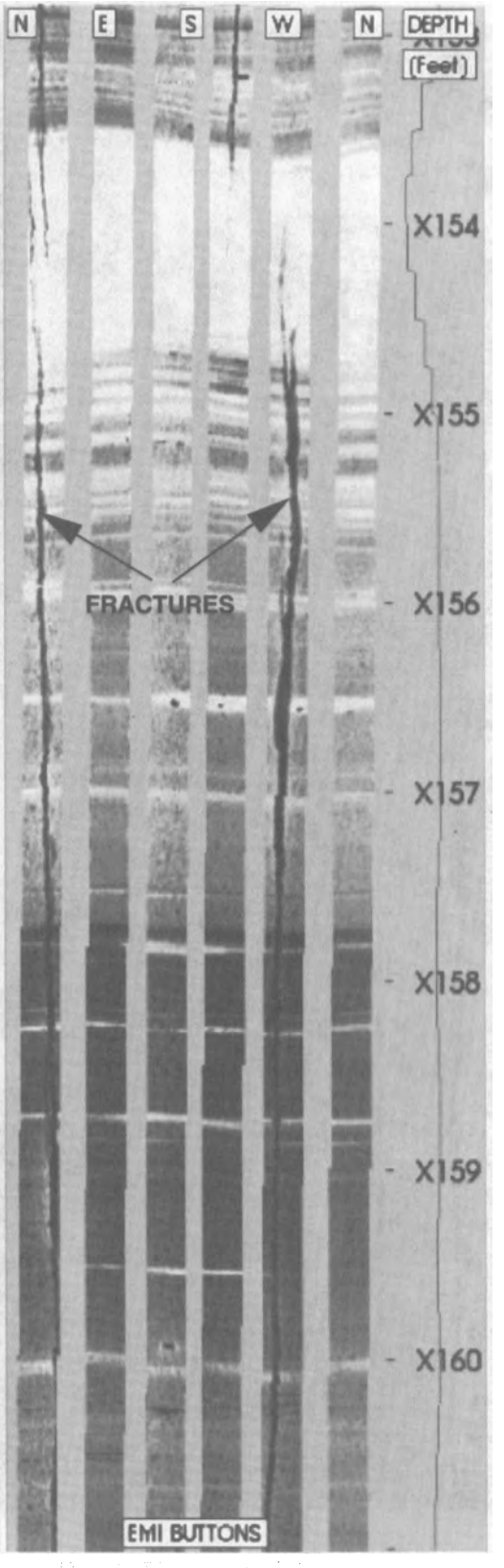

Fig. 4 Electrical Micro–Imaging display.

Density/Neutron of the Canyon Reef

Figure 5 not available.

Fig. 5 Conventional logging suite underestimating actual production results

EMI display of the porosity break zone

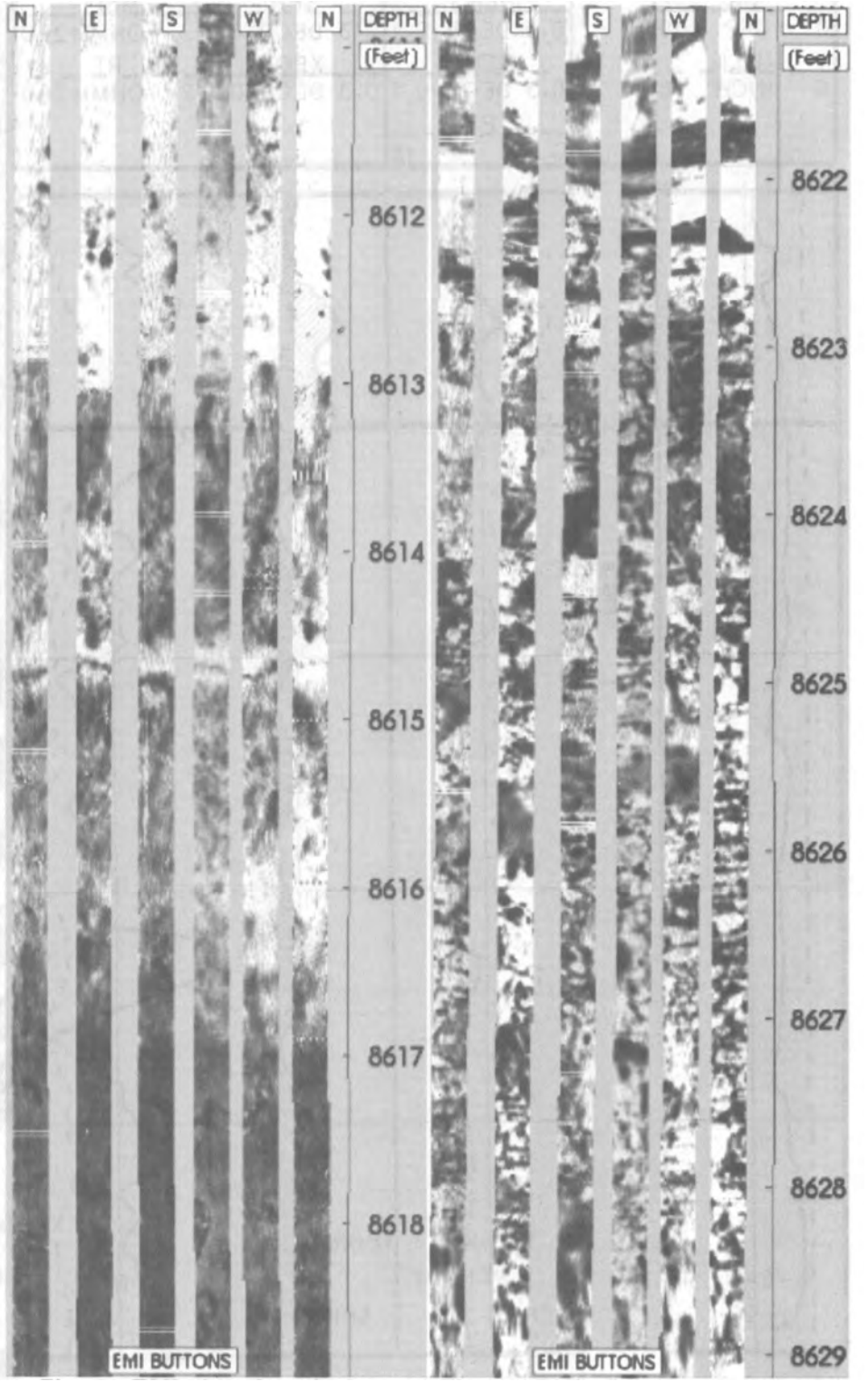

Fig. 6a EMI showing darker band as matrix porosity.

EMI display of the complex network of secondary porosity

Fig. 6b EMI shows network of interconnected porosity.

Standard porosity / resistivity logs of the Clearfork formation

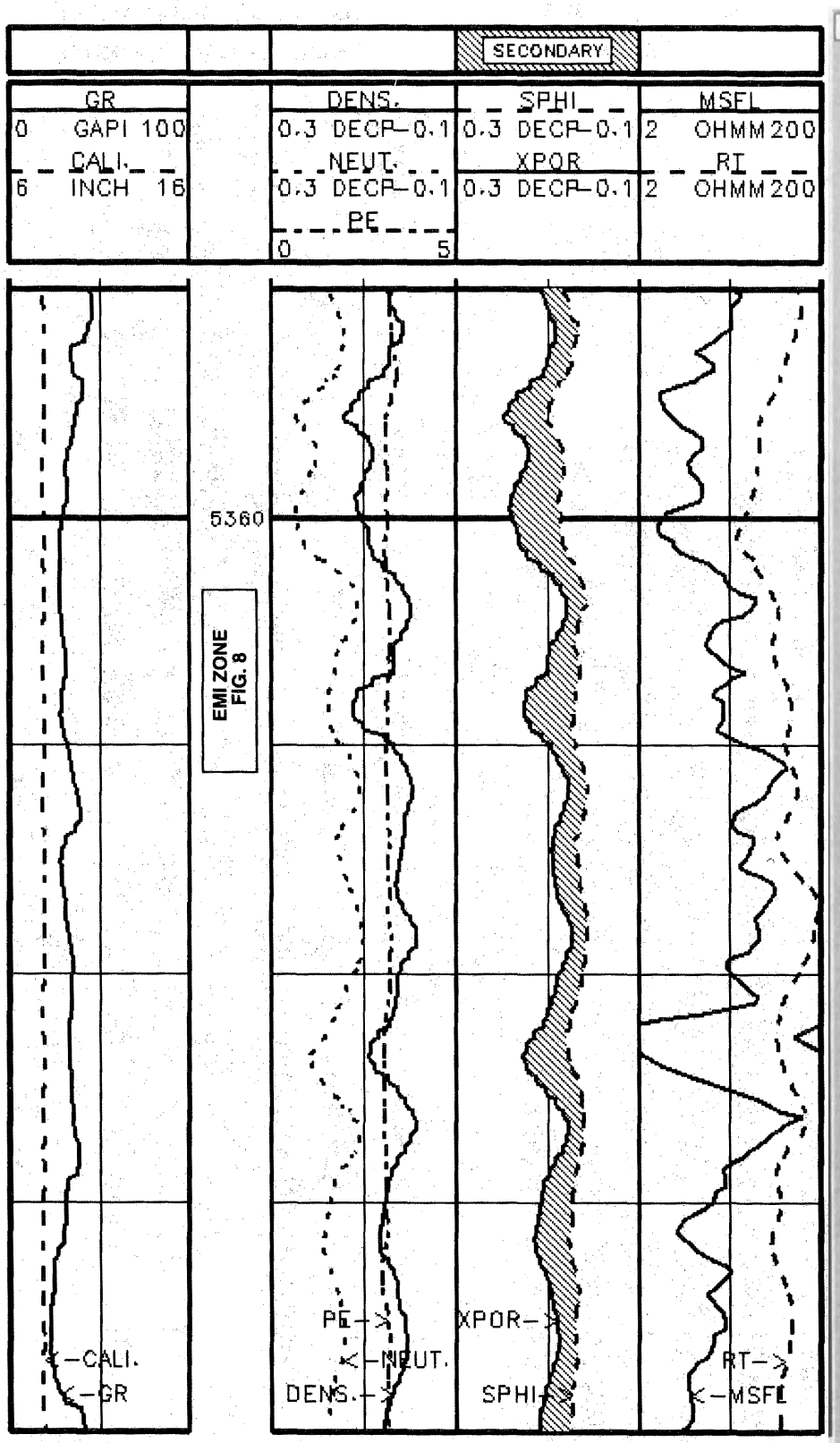

Fig. 7 Neutron–density crossplot porosity is twice the value of the mean sonic porosity suggesting secondary porosity.

EMI display of a vugular secondary porosity

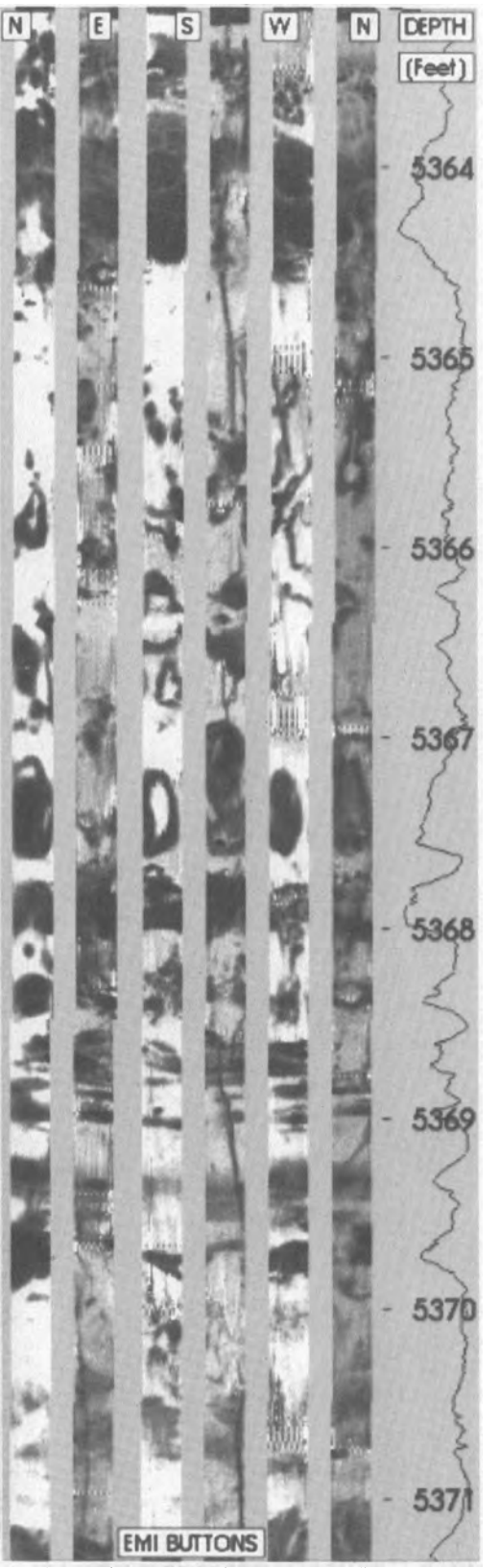

Fig. 8 EMI shows pore geometry of vugular formations.